

High Speed Stereoscopic Shadowgraph and Its Digital 3D Reconstruction

Q Wang (✉) and Y Zhang

Department of Mechanical Engineering, University of Sheffield,
Mappin Street, Sheffield, S1 3JD, UK

1. Introduction

Schlieren/shadowgraph technique remains to be one of the powerful flow visualisation techniques due to their relatively easy implementation, high and variable sensitivity, low cost and the use of conventional light sources [1]. Schlieren/shadowgraph has been applied widely to study combustion [2, 3], aerodynamics [4, 5], fluid mechanics [6, 7], etc. Schlieren and shadowgraph are closely related and developed together, but there are several distinctions between them. First, schlieren methods require a knife edge to cut off the refracted light, but no such cutoff is needed in shadowgraph. Second, the illuminance level in a schlieren image responds to the first spatial derivative of the refractive index in the test field, while shadowgraph responds to the second spatial derivative of the refractive index. Equivalently, the schlieren image displays the deflection angle while shadowgraph displays the ray displacement resulting from the deflection. Finally, schlieren is more sensitive than shadowgraph in general and could be applied on weaker disturbances. However shadowgraph is able to show the salient features of a subject without gross changes in illumination. Thus the application of schlieren or shadowgraph depends on the actual characteristics of the test field and the objective of the investigation.

However, in conventional schlieren/shadowgraph technique, the resultant image is integration along the optical path. The in depth information has been lost. Stereoscopic schlieren techniques have been attempted in the middle of the 20th century to overcome this shortcoming. A stereoscopic method was used by Lyot and Franconfor to examine glass discs [8], by taking photos from two different directions with a single parallel beam in sequence. Due to the time delay between the two images, it is not suitable for unsteady phenomena. In order to take photographs from two directions simultaneously, two inclined beams were formed with two pair of lenses for the investigation of aerodynamics [9]. The stereoscopic schlieren system setup by John H. Hett [10], consisting of a pair of parabolic mirrors and 10 flat mirrors, was also able to take two images at two directions simultaneously. Besides the complicated apparatus of this system, the test section was much smaller than the parabolic mirror diameter. The technique had been applied to combustion research consequently and was able to observe the flame development at two directions simultaneously. However, the test sections of the stereoscopic schlieren systems mentioned above were all in the common area of the two parallel beams. Thus although two images could be recorded at different directions, the images do not satisfy the characteristics of projective geometry. Strictly speaking, the techniques are not real 'stereoscopic'.

Stereoscopic, or 3D photography, works because it is capable of creating the illusion of depth in an image by presenting a slightly different image to each eye. If one takes two separate photographs that same distance apart, with a suitable viewer it is possible to recreate the illusion of depth by human brain. Modern industry and research apply stereoscopic technology to detect and record 3D information based on projective geometry. The depth information can be reconstructed from two images through camera calibration and corresponding points extracted from the two images. Recently, Ng [11] applied the stereoscopic methodology to reconstruct and visualise the 3D surface topology of turbulent diffusion flames. Their experiments were carried out using only the basic stereo apparatus of a high-resolution digital camera and a stereo adapter. The 3D surface could be reconstructed and observed, which provides the quantitative in depth information.

Considering the great progress both in digital imaging and image processing, it inspires the idea to explore the stereoscopic schlieren/shadowgraph technique with modern high speed cameras. Rather than observing the 3D images in a stereoscope, the quantitative in depth information could be

extracted digitally through 3D reconstruction. In this paper, a stereoscopic shadowgraph system is established using conventional z-type schlieren system. The 3D system is applied to investigate the hot gas jet generated by a gas turbine igniter successfully. The obtained image pairs are then analysed by the 3D digital reconstruction algorithm developed for the 3D stereoscopic system.

2. Experimental setup

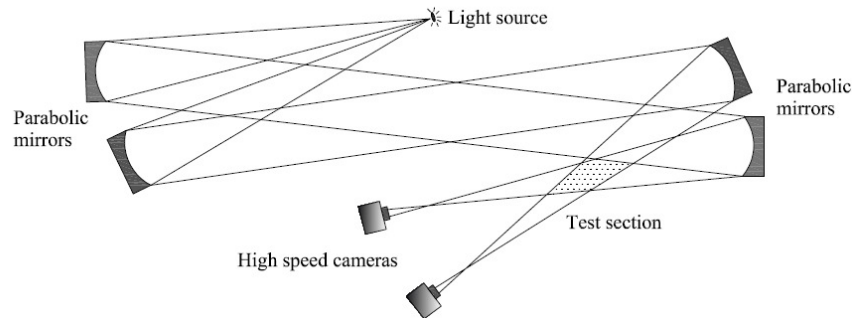


Fig. 1 Schematic illustration of the stereoscopic shadowgraph system

The schematic apparatus of the stereoscopic shadowgraph system is shown in Fig.1. The system consists of four parabolic mirrors, forming two inclined light beams. The light source is a 500 W Xenon lamp. The $\lambda/10$ parabolic mirrors are 0.3048 m (12 inches) in diameter and 3.048 m (10 feet) in focal length. Two high speed cameras (Photron SA3) are used to record the shadowgraph images simultaneously. The converging light beams project on the camera focal planes directly. Since the stereo calibration algorithm is based on projective geometry, the test section of the stereoscopic shadowgraph system is placed at the crossing volume of the two converging beams rather than the parallel beams. A gas turbine combustor igniter was placed in the test section under investigation.

Camera calibration is a necessary step to extract metric information from 2D images. The proposed technique established by Zhang [12] is utilized in this study. The calibration is flexible, robust and low cost. It only requires a planar pattern at a few different orientations and the motion of the planar patterns need not be known. Combined with the known calibration parameters and the corresponding points in the stereo images, 3D coordinates could be established. A calibration board with 64 identical square holes obtained by accurate acid etching on a thin steel plate is used for the calibration parameters estimation. The error of calibration parameters is less than 2%.

3. Basic Equations for Camera Calibration and 3D Reconstruction

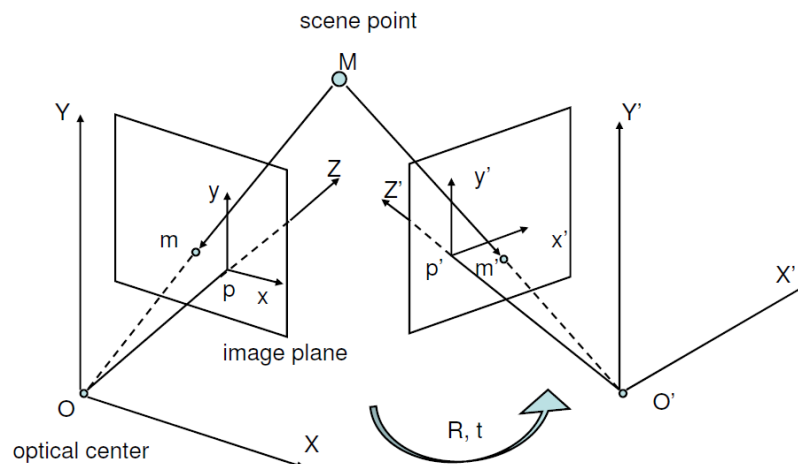


Fig. 2 Physical and image coordinates

Figure 2 shows the physical coordinates of the scene point in the test section and the image coordinates on the image plane. The relationship between the two coordinates satisfies the principles of projective geometry. In projective camera model, a 2D point is denoted by $m = [u, v]^T$. A 3D point is denoted by $M = [X, Y, Z]^T$. The augmented vector is denoted by adding 1 as the last element: $\tilde{m} = [u, v, 1]^T$ and $\tilde{M} = [X, Y, Z, 1]^T$. As shown in Fig.2, the camera is reduced to a point and an image plane. Points in the world coordinates form rays by connecting the optical centre and project images on the image planes. The relationship between a 3D point M and its image projection m is given by

$$s\tilde{m} = A[R \quad t]\tilde{M}, \text{ with } A = \begin{bmatrix} \alpha & \gamma & u_0 \\ 0 & \beta & v_0 \\ 0 & 0 & 1 \end{bmatrix}, \quad (1)$$

Where s is an arbitrary scale factor, (R, t) , called the extrinsic parameters, the rotation and translation relating the world coordinate system to the camera coordinate system. A is called the camera intrinsic matrix, with (u_0, v_0) the coordinates of the principal point p , α and β the scale factors for u and v in image, and γ the parameter describing the skew of the two image axes.

In stereo reconstruction methods, two camera systems are used. We designated one camera coordinate as the world coordinate and the other camera coordinate is related to the world coordinate via the extrinsic parameters (R, t) . Then we have

$$\tilde{m}_i = P\tilde{M}_i = A[I \quad 0]M_i \quad (2)$$

$$\tilde{m}'_i = P'\tilde{M}_i = A'[R \quad t]M_i. \quad (3)$$

Without loss of generality, we assume the model plane is on $Z = 0$ of the world coordinate system. Let's denote the i^{th} column of the rotation matrix R by r_i . From Eq. 1, we have

$$s \begin{bmatrix} u \\ v \\ 1 \end{bmatrix} = A[r_1 \quad r_2 \quad r_3 \quad t] \begin{bmatrix} X \\ Y \\ 0 \\ 1 \end{bmatrix} = A[r_1 \quad r_2 \quad t] \begin{bmatrix} X \\ Y \\ 1 \end{bmatrix}. \quad (4)$$

We still use M to denote a point on the model plane, but $M = [X, Y]^T$ since Z is always equal to 0. In turn, $\tilde{M} = [X, Y, 1]^T$. Therefore, a model point M and its image m is related by a homography H :

$$s\tilde{m} = H\tilde{M} \quad \text{with } H = A[r_1 \quad r_2 \quad t]. \quad (5)$$

Given an image in which image coordinates can be measured and a model plane whose coordinates are already known, a homography can be estimated. Let's denote it by $H = [h_1 \quad h_2 \quad h_3]$. From Eq. 4, we have

$$[h_1 \quad h_2 \quad h_3] = \lambda A[r_1 \quad r_2 \quad t], \quad (6)$$

where λ is an arbitrary scalar. Using the knowledge that r_1 and r_2 are orthogonal, we have

$$h_1^T A^{-T} A^{-1} h_2 = 0 \quad (7)$$

$$h_1^T A^{-T} A^{-1} h_1 = h_2^T A^{-T} A^{-1} h_2. \quad (8)$$

These are two basic constraints on the intrinsic parameters, given one homography. As the DoF of the intrinsic matrix is 5, therefore at least $n \geq 3$ homographies from n images are needed to provide a unique solution of the intrinsic parameters.

By elimination of M in Eq.2 and Eq.3, the following fundamental equation is obtained

$$\tilde{m}_i^T A^{-T} T R A^{-1} \tilde{m}_i = 0, \quad (9)$$

where T is the skew-symmetric matrix defined by t . Equation 9 characterizes the extrinsic parameters in terms of measured corresponding image points.

Metric reconstruction of the scene is possible with the intrinsic and extrinsic parameters obtained by linear triangulation methods. According to Eq.2 and Eq.3, the two projective matrixes P and P' for the two cameras can be rewritten in the form

$$\begin{bmatrix} x_1 P_{13}^T - P_{11}^T \\ y_1 P_{13}^T - P_{12}^T \\ x_2 P_{23}^T - P_{21}^T \\ y_2 P_{23}^T - P_{22}^T \end{bmatrix} \tilde{M} = B \tilde{M} = 0 \quad (10)$$

where $\{(x_i, y_i) | i=1,2\}$ are the Euclidean coordinates of image points (m_1, m_2) and P_{ij} ($i=1,2; j=1,2,3$) is the j^{th} row of the projective matrix P_i . However, there are only three unknowns in $\tilde{M} = (X, Y, Z, 1)^T$, the over determined set of equations can be solved by least squares technique.

4. Results and discussions

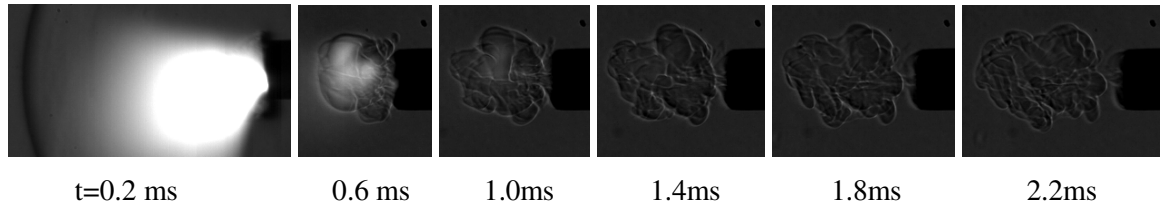


Fig.3 Shadowgraph sequence of spark induced hot gas propagation

In the experiments, the spark was only generated in ambient air, without fuel mixture around. A sequence of conventional shadowgraph images of the spark initiation were illustrated in Fig. 3. After the spark initiation, a light flash is observed with a sharp acoustic sound and the electrical spark induced shockwave was captured successfully. A hot gas jet is observed propagating along the igniter axis in the shadowgraph image sequence.

From Fig.3, it could be observed that the interaction between the hot gas and ambient air is turbulent and has irregular structures. The stereoscopic shadowgraph technique is then applied to investigate the 3D structure of the hot gas. Figure 4a gives a sample pair of stereoscopic shadowgraph images. The features in the images show the interactions between the hot gas and ambient air. With careful examination, it could be observed that the curves in the two images are different in detail structure. The standard stereo matching techniques which employ dense disparity matching are used to extract the correspondence points in the image pairs. The method works quite well on surfaces with texture or being non-smooth. However, the correlation approach tends to fail in smooth surfaces without features. The correspondence points extracted are plotted in Fig. 4b. The main features of the interaction interfaces are extracted successfully. With the calibration parameters given, corresponding feature points from the image pairs can be reconstructed. The raw data does not really describe

surfaces, but only clouds of point coordinates in three-dimensional space. A three-dimensional mesh is applied to represent the 3D structure.



Fig. 4 (a) A sample pair of stereoscopic shadowgraph images ($t=2.2\text{ms}$)
 (b) Correspondence points selected for reconstruction

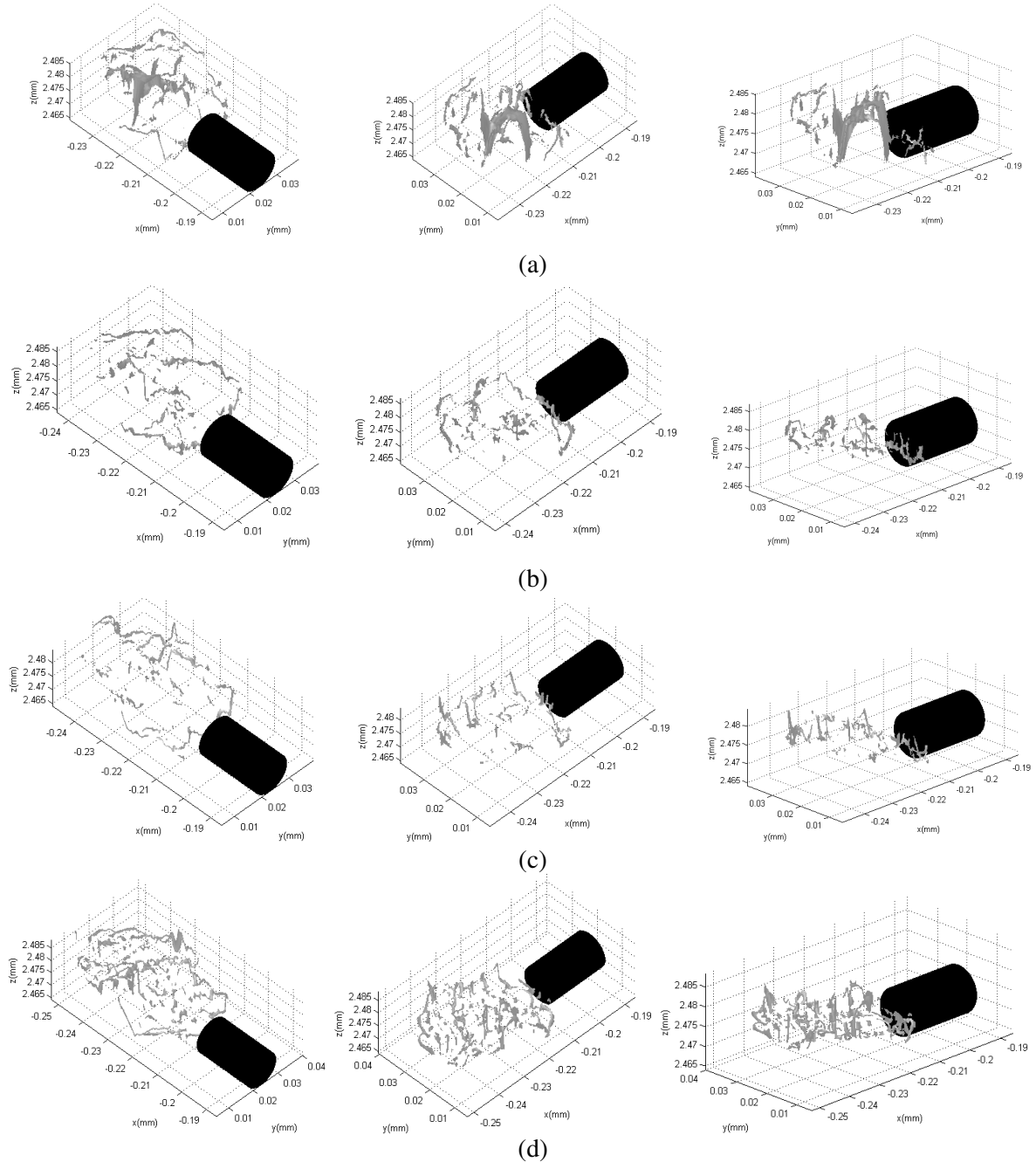


Fig.5 3D views of reconstructed structure at (a) $t=1.0$ ms, (b) $t=1.4$ ms, (c) $t=1.8$ ms, (d) $t=2.2$ ms

The 3D structure of the hot gas and ambient air interaction interfaces are illustrated in Fig.5. The 3D shape and distribution of salient features are extracted from the stereoscopic shadowgraph image pairs successfully. The irregular structures shown in Fig. 5 could only be well understood through different 3D views. Any observation only depending on 2D structure is not sufficient and may even mislead. The 3D reconstruction ability of the stereoscopic shadowgraph method proposed in this study thus has great advantages over conventional 2D schlieren/shadowgraph techniques. The 3D structure is of great help to understand the hot gas kernel development, which are difficult to be accomplished by other conventional techniques.

5. Conclusions

A stereoscopic shadowgraph system has been established with two pairs of parabolic mirrors. The system is calibrated based on projective geometry. A steel calibration board manufactured by accurate acid method is used for the calibration.

The advantage of the stereoscopic system is to extract the quantitative depth information and thus to reconstruct the 3D coordinates of the object from two shadowgraph images. The method has acted as a bridge to combine stereo and shadowgraph successfully. Thus it broadens the application of stereo technique and improves the capability of shadowgraph technique. The technique is able to reconstruct the 3D structures in a specific volume rather than only on a surface such as stereoscopic PIV. The synchronization of the two high speed cameras makes it possible to get time resolved results of unsteady phenomenon. In this study, the time resolved 3D features of an electrical spark initiation process has been extracted successfully.

Acknowledgement

Q. Wang would like to thank the University of Manchester, the University of Sheffield and BP Alternative Energy International Ltd for providing PhD scholarships during which part of this research work was carried out. This research is further supported by EPSRC through the Grant No. EP/G063044/1.

References

- [1] Settles, G.S. (2002). *Schlieren and Shadowgraph Techniques*. Springer-Verlag Berlin Heidelberg New York (ISBN 3-540-66155-7).
- [2] Davis, M.R. and P. Rerkshanandana. (1993). Schlieren measurement of turbulent structure in a diffusion flame. *Exp. Therm. Fluid Sci.* 6: 402.
- [3] Strozzi, C., et al.(2008). Experimental and numerical study of the influence of temperature heterogeneities on self-ignition process of methane-air mixtures in a rapid compression machine. *Comb. Sci. and Tech.* 180: 1829.
- [4] Settles, G.S. (1985). Colour-coding schlieren techniques for the optical study of heat and fluid flow. *Int. J. Heat Fluid Flow.* 6: 3.
- [5] Kleine, H. and H. Gronig. (1991). Color schlieren methods in shock wave research. *Shock Waves.* 1: 51.
- [6] Fiedler, H., et al. (1985) Schlieren photography of water flow. *Exp. Fluids.* 3: 145.
- [7] Peters, F., T. Kuralt, and J. Schniderjan. (1992). Visualization of water flow by sugar schlieren. *Exp. Fluids.* 12: 351.
- [8] B. Lyot, M.F. (1948) Observation des défaut de poli et homogénéité au stéréoscope par la méthode du contraste de phase. *Revue Optique.* 27.
- [9] Veret, C. (1952). La strioscopie stéréoscopique *La Recherche Aeronautique.* 29.
- [10] Hett, J.H. (1951). A high-speed stereoscopic schlieren System. *J. Soc. Motion Picture Engineers,* 56.
- [11] Ng, W.B. and Y. Zhang. (2003). Stereoscopic imaging and reconstruction of the 3D geometry of flame surfaces. *Exp. Fluids.* 34: 484.
- [12] Zhang, Z. (2000). A flexible new technique for camera calibration. *IEEE TPAMI.* 22: 1330.